2002

A Collaborative Numerical and Experimental Investigation of Flapping-Wing Propulsion

Jones, K.D.; Castro, B.M.; Mahmoud, O.; Pollard, S.J.; Platzer, M.F.; Neef, M.; Gonet, K.; Hummel, D.

Jones, K.D., Castro, B.M., Mahmoud, O., Pollard, S.J., Platzer, M.F., Neef, M., Gonet, K. and Hummel, D., "A Collaborative Numerical and Experimental Investigation of Flapping-Wing Propulsion," AIAA Paper No. 2002-0706, Reno, Nevada, Jan. 2002.
https://hdl.handle.net/10945/37200

AIAA−2002−0706

A COLLABORATIVE NUMERICAL AND EXPERIMENTAL INVESTIGATION OF FLAPPING−WING PROPULSION

K.D.Jones, B.M. Castro, O. Mahmoud,
S.J. Pollard and M.F.Platzer
Naval Postgraduate School
Monterey, CA

M.F. Neef, K. Gonet and D. Hummel
Institut für Strömungsmechanik
TU Braunschweig, Germany

40th Aerospace Sciences Meeting & Exhibit
14−17 January 2002 / Reno, NV

A COLLABORATIVE NUMERICAL AND EXPERIMENTAL INVESTIGATION OF FLAPPING-WING PROPULSION

K. D. Jones[a], **B. M. Castro**[b], **O. Mahmoud**[b], **S. J. Pollard**[b] **and M. F. Platzer**[c]
Naval Postgraduate School
Monterey, California

M. F. Neef[d], **K. Gonet**[e] **and D. Hummel**[f]
Institut für Strömungsmechanik
TU Braunschweig, Germany

Abstract

An international, collaborative investigation is undertaken to evaluate the relative merits and limitations of various numerical methods and experimental measurement techniques, specifically for the analysis of flapping-wing propulsion. A finite aspect-ratio configuration is extensively investigated, both quantitatively and qualitatively, in a low-speed wind tunnel. Direct force measurements are made, as well as time-accurate and time-averaged laser Doppler velocimetry and unsteady flow visualization. The reduced frequency, mean angle of attack, aspect ratio and Reynolds number are varied in the experiments. The experiment is numerically simulated using flat-plate theory, two and three-dimensional panel codes, and two and three-dimensional Euler and Navier-Stokes solvers. The ability of each of the methods to capture important aspects of the flow physics are evaluated through comparisons with each other and the experimental data. Additionally, the comparisons indicate areas where further research is needed. The collaborative effort provides a survey of available capabilities and provides a fixed set of flapping-wing data for others to compare against.

[a] Research Assistant Professor, Senior Member, AIAA
[b] Graduate Student, Student Member, AIAA
[c] Professor, Fellow, AIAA
[d] Graduate Student
[e] Student
[f] Professor, Associate Fellow, AIAA

Nomenclature

a	= speed of sound
A	= aspect ratio, b/c
b	= wing span
c	= chord length
C_D	= drag coefficient, Drag$/(q_\infty S)$
$C_{D\,\mathrm{stat}}$	= drag coefficient of the non-moving airfoil
C_L	= lift coefficient, Lift$/(q_\infty S)$
C_T	= thrust coefficient, $-C_D + C_{D\,\mathrm{stat}}$
C_P	= power coefficient, $-C_L \dot{z}/U_\infty$
f	= frequency in Hertz
f'	= factor for calculating lift
h	= plunge amplitude in terms of c
k	= reduced frequency, $2\pi f c/U_\infty$
l	= length scale
$\mathbf{M}$	= Mach number
q	= dynamic pressure, $\rho U^2/2$
Re	= chord Reynolds number, $U_\infty c/\nu_\infty$
S	= wing area, bc
Sr	= Strouhal number, $lk/(2\pi)$
t	= time
T	= nondimensional time per period, $2\pi/k$
U	= horizontal velocity
u'	= factor for calculating induced drag
x, y, z	= Cartesian coordinates in terms of c
$z(\tau)$	= vertical displacement in terms of c
α	= mean angle of attack
η	= propulsive efficiency, $\overline{C}_T/\overline{C}_P$
ν	= kinematic viscosity
ρ	= density
τ	= nondimensional time, tU_∞/c
$(\dot{})$	= rate of change with respect to τ
$(\bar{})$	= averaged over one period T
$(\,)_\infty$	= free-stream value

I. Introduction

The agile flight of birds and insects has been an inspiration to scientists for many centuries. However, since the first part of the 20th century, little effort has been directed toward understanding and exploiting the aerodynamics demonstrated by these creatures. The lack of industrial applications has relegated the study of flapping-wing flight to something of a *hobby-like* status, with very little research funding available for serious investigations, with most notable progress made by model airplane enthusiasts. However, recent interest in small, unmanned air vehicles (UAVs) and micro air vehicles (MAVs) have led to a renewed interest in flapping-wing propulsion, and an influx of research funds. The ability of the dragonfly to hover and maneuver in confined areas, as well as to achieve high speeds and to fly in turbulent air has drawn significant interest, but has as yet proved to be a formidable goal for scientists to duplicate numerically or mechanically.

These vehicles operate at very low Reynolds numbers, from a few hundred to a few tens of thousands, and they encounter, and even benefit from, massive flow separation over a large part of the flapping cycle. Historically, little effort has been given to the development of numerical flow solvers suitable for this flight regime, and very little experimental data has been generated for the validation of the numerical methods. Thus, the primary goal of the present collaborative effort is to thoroughly investigate a generic flapping-wing configuration, both experimentally and numerically, using a variety of methods to obtain quantitative and qualitative data, providing something like a *benchmark* study in flapping-wing aerodynamics.

Most of the present authors have been involved in unsteady aerodynamics, and many have performed studies of flapping-wing propulsion. At the Naval Postgraduate School, Jones and Platzer investigated propulsion and power-extraction using a two-dimensional unsteady panel method [1]. Jones *et al.* [2] performed flow-visualization and LDV experiments in a water tunnel, and compared the results with the panel method. Jones and Platzer [3], Lund [4] and Jones *et al.* [5] developed a flapping-wing model for testing in a low-speed wind-tunnel, and compared direct thrust measurements to the panel method for several configurations. Jones and Platzer [6], Duggan [7] and Jones *et al.* [8] developed $15cm$ length/span MAV models and compared direct thrust measurements and flow visualizations to the panel method. A two-dimensional, unsteady Navier-Stokes solver was developed and tested for a number of unsteady problems including flapping-wing propulsion, flutter and dynamic stall [9–11].

At the Institute of Fluid Mechanics of the Technical University of Braunschweig, various aspects of bird flight have been investigated, mainly focusing on slotted wing-tips [12], formation flight [13] and the aerodynamics of tails in birds [14]. While a first approach to flapping flight for comparison with experimental data was already made in 1977 [15], a detailed study of the unsteady aerodynamics around moving wings has recently become accessible by the use of Computational Fluid Dynamics (CFD) and the development of a three-dimensional, Euler/Navier-Stokes solver (FLOWer). Experience in unsteady flows was gathered by the numerical calculation of the vortex breakdown over a delta wing [16]. Application of the code to moving surfaces has led to the solution of the Euler-equations for the flow around a flapping and twisting wing [17], which has also been extended to viscous flows.

In the present investigation, a relatively simple, finite aspect-ratio configuration is chosen, and extensive experimental measurements and numerical simulations are made, and the results are compared both qualitatively and quantitatively, highlighting the strengths and weaknesses of the various methods.

II. Approach

In the following sections, the geometry of the flapping-wing configuration, the flapping-motion and the parameter-space are defined. The experimental and numerical methods utilized are described briefly with references for more detailed descriptions of the methods and references for validation studies.

Configuration

A single, finite aspect-ratio wing is flapped sinusoidally with a pure-plunge motion in a parallel manner (i.e. the plunge amplitude is constant in the span-wise direction), with the motion defined by

$$z(\tau) = h\cos(k\tau). \tag{1}$$

All numerical calculations have been carried out assuming a NACA 0014 airfoil section, which closely approximates the wing on the experimental model. A plunge amplitude of $h = 0.4c$ was chosen for all cases, which is also the maximum amplitude of the experimental model. The configuration with the relevant parameters is shown in Fig. 1.

The parameter-space for the investigation includes the reduced frequency, k, the aspect ratio, A, and

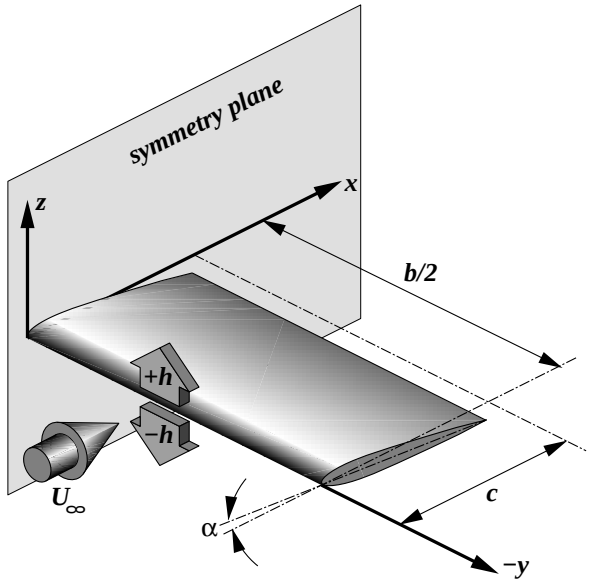

Fig. 1: Flapping-wing geometry and parameters

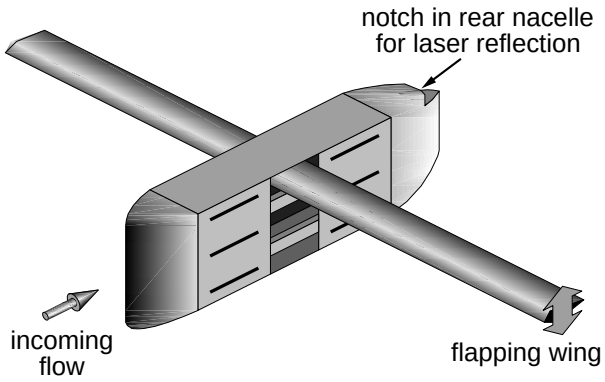

Fig. 2: Isometric view of the model

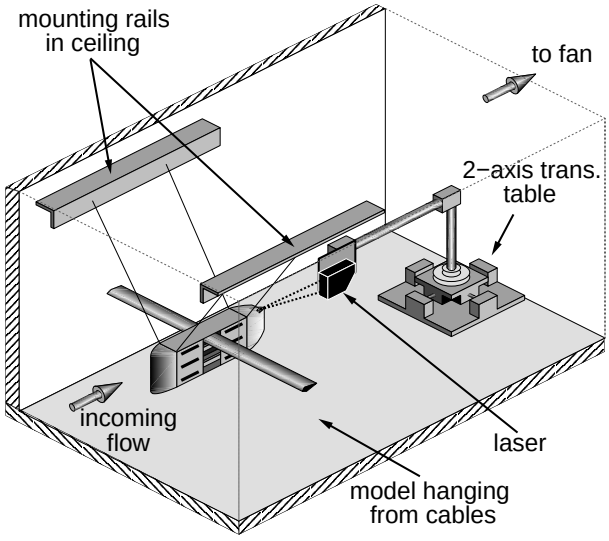

Fig. 3: The model mounted in the test-section

the mean angle of attack, α, which is assumed to be zero if not otherwise stated. Experimentally, a given reduced frequency may be achieved through an infinite variation of dimensional frequency and flow speed, providing some measure of the Reynolds number sensitivity. Similarly, the Navier-Stokes solvers also allow for the specification of the Reynolds number as well as the Mach number. While the compressible Euler/Navier-Stokes solvers are not capable of operating at the very low Mach number of the experiment (< 0.03), all simulations are performed for $0.1 < \mathbf{M}_\infty < 0.3$. All presented numerical data are taken several cycles into the simulation, after transients have diminished and periodic behavior is obtained. Note, in some of the low Reynolds number simulations, where shedding and separation are predominant, periodicity is often not achieved, but rather the solution follows an attractor.

Experimental Approach

The experimental flapping mechanism was previously developed by Jones and Platzer [3], originally as a bi-plane (or *wing flapping in ground-effect*) configuration. For the present investigation, only a single flapping wing is considered, and consequently the second wing on the model is removed, and replaced with a counter weight to minimize model vibrations. An isometric view of the model is shown in Fig. 2.

In previous investigations (Refs. [3,4]) only thrust measurements were made, utilizing the pendulum arrangement shown in Fig. 3. The model was suspended from the tunnel ceiling using four cables such that it could swing freely in the streamwise direction, but remained stable in all other directions. When drag or thrust was generated, the model was displaced in the streamwise direction. The displacement was measured using a very accurate laser range finder in a fixed position downstream of the model, and the thrust was calculated from a calibration curve.

In summary, the model flaps a wing sinusoidally in plunge. The wing has a chordlength of 64 mm and a maximum span of 1200 mm, with 89 mm taken up by the body at the center, resulting in a maximum effective aspect ratio of 17.4. Lower aspect ratios are tested using shorter span wings. Flapping-frequencies up to about 8 Hz are possible with the present gearing. The frequency is usually set using a strobe light, but the actual value, as well as the fluctuations, are measured using a rotary motion encoder mounted in the model.

Testing is performed in the Naval Postgraduate School 1.5 × 1.5 m low-speed wind tunnel, a con-

tinuous, flow-through facility, with a 9:1 contraction ratio and a maximum speed of about 9.5 m/s. Turbulence levels in the test section were measured by Lund [4] using LDV, and were found to be less than 1.75 percent for speeds above 1.5 m/s. Chord-Reynolds numbers up to 4.5×10^4 are possible, but most experiments were performed at $1.0 \times 10^4 < Re < 4.0 \times 10^4$.

The tunnel has been fitted with an unsteady LDV system, and both time-accurate and time-averaged velocity measurements have been made. The TSI LDV system uses a Coherent Innova Argon-Ion $5W$ laser, and the signal is processed through an IFA 755 processor and the FIND software package. Unsteady signals are encoded using a TSI 1989A high-speed Rotating Machinery Resolver (RMR) which has a Once Per Revolution (OPR) capability of 200 to 120,000 RPM, with a 0.1 degree resolution, and selectable locking detection of ± 96 min to ± 768 min of arc. The PACE software is used to interface with the RMR and LDV. Flow seeding is performed using a TSI 9306 six-jet atomizer, operating with compressed air. Distilled water is used in place of glycerin oil, as it produces more particles, approximately 1 micron in size. More details are given in Ref. [18].

Flow visualization is presently performed in the wind tunnel using a smoke wire. The smoke wire is constructed from a length of 0.25 mm diameter Nickel Chromium (Ni80/Cr20) wire stretched between two posts. Roscoe smoke fluid is dripped down the wire, and when current is run through the wire, it is heated, and the fluid burns off providing a smoke sheet for a few seconds. By wrapping and soldering bands of 0.13 mm diameter copper wire around the NiCr wire at 10 mm intervals, the fluid pools on the bands and then burns for a longer time, providing 10 to 15 seconds of narrow streaklines. Fluid is delivered to the wire via vinyl tubing from a pressurized reservoir. The smoke wire is useful in the range $1 \leq U_\infty \leq 3$ m/s which corresponds to $0.5 \times 10^4 < Re < 1.5 \times 10^4$. If the speed is too low, the heated smoke rises creating an apparent angle of attack. If the Reynolds number based on the wire diameter is greater than about 40, the wire starts to shed a vortex street, which rapidly dissipates the streaklines due to turbulent mixing.

Numerical Approach

A broad assortment of numerical methods have been utilized in this study. The methods range from flat-plate theory, providing results instantaneously, to three-dimensional Navier-Stokes simulations, requiring several hours of super-computer time.

Two-Dimensional Theory In the 1930's, Garrick [19] extended Theodorsen's [20] flat-plate theory to compute the streamwise force on a wing. At about the same time, Küssner [21] developed a similar method as an extension to Birnbaum's [22] earlier work, yielding identical results to Garrick's method. Both methods assume that the airfoil is a flat-plate undergoing sinusoidal oscillations of relatively small amplitude and, consequently, that all shed vorticity convects downstream in the plane of the airfoil. It's important to note that this restriction means that the wake can only yield a normal force on the airfoil. The methods utilize a so-called *lift-deficiency* function, given as tabular values derived using Bessel functions. Aerodynamic forces are computed from the tabular function by solving simple algebraic functions, and require very little computational effort.

Three-Dimensional Theory While no three-dimensional unsteady theory applicable to this study was readily available, approximations for the limiting cases can be made. As the flapping frequency goes to zero, the plunge velocity becomes small, and the three-dimensional propulsive efficiency is approximated by

$$\eta_{k \to 0} = 1 - \frac{2f'}{(A+2)u'} \tag{2}$$

where f' and u' are factors for the calculation of lift and induced drag. Their values for a non-tapered, non twisted rectangular wing of aspect ratio $A = 4$, 8 or 20 are given by Abbott and von Doenhoff [23].

As the frequency increases, the wake-wavelength diminishes. Consequently, it can be argued that the effect of the oscillatory trailing tip-vortices on the wing diminishes due to vorticity cancellation. In the limit for large k, the tip vortices would not induce a down-wash at all, as an infinite series of alternating-sign vortices should be coincident at the tip and, thus, at high frequencies the performance would be independent of the aspect ratio, reducing to the two-dimensional case.

Two-Dimensional Panel Code An unsteady panel code originally developed by Teng [24] with additional features and a graphical user interface (GUI) developed by Jones and Center [25] is used for two-dimensional potential-flow solutions. The basic approach follows the method of Hess and Smith [26], with the vorticity shedding procedure of Basu and Hancock [27] for unsteady simulations.

The code employs a deforming wake model, where a discrete vortex is shed from the trailing edge at the

end of each time step to account for the change in circulation about the airfoil. These vortices convect downstream, influencing each other and the airfoil, providing an accurate model of wake roll-up. For academic purposes, the deforming-wake model may be disabled, such that the wake resembles the wake used by the flat-plate theory. Details of the code and validation can be found in the references cited above as well as in Refs. [1–3].

In this study, the airfoil surface was represented by 200 panels, 120 time-steps per cycle were used, and the solutions were run for 6-10 cycles, or until the transients vanished. The code is run on PC's or workstations, and requires a few minutes per solution.

Three-Dimensional Panel Code Three-dimensional potential-flow simulations are performed with CMARC, the flow-solving module from the Digital Wind Tunnel (DWT) software suite from AeroLogic [28, 29]. CMARC is a PC-based version of PMARC (Panel Method Ames Research Center), a low-order, 3D panel code.

Only the right wing is modeled due to the $x-z$ plane of symmetry. All wing models have 20 chord-wise and 20 semi-span-wise panels, plus 40 panels to model the *body-of-revolution* wingtip, for a total of 440 panels. Panels are distributed with half-cosine spacing along the span, with the tightest spacing at the tip, and full-cosine spacing in the chord-wise direction. Typically 100 steps/cycle are used in a simulation. The grid of the $A = 8$ wing is shown in Fig. 4, with both the right and the reflected left-wing shown.

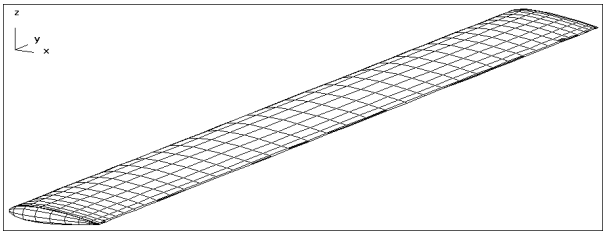

Fig. 4: Full wing for the 3D panel code, $A = 8$

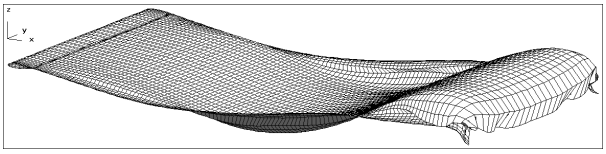

Fig. 5: Wake after 1 cycle (3D panel), $k = 0.4$, $A = 8$

Both rigid and deforming wake models are available, and while the rigid wake model is generally more stable for higher frequency simulations, the deforming wake model provides a more accurate model of the unsteady wake topology, as well as a more accurate prediction of aerodynamic forces, hence the deforming wake model is used here. The deforming wake after the first cycle is illustrated in Fig. 5 for $k = 0.4$, $A = 8$.

To test for panel convergence, the number of panels in the span-wise and chord-wise directions was doubled, with minimal change in the integrated values. The presented results were obtained running the code on a Pentium III 500MHz PC, which typically required a few hours to compute 3 cycles.

NSTRANS A two-dimensional, unsteady, compressible Euler/Navier-Stokes solver (NSTRANS) was developed at the Naval Postgraduate School. The algorithm was originally developed by Ekaterinaris and Menter [30], using Osher's third-order accurate, upwind scheme [31, 32], Steger-Warming flux-vector splitting [33] for linearization of the left-hand-side, and second-order central differences for computation of the viscous fluxes. Time accuracy was improved by performing Newton sub-iterations to convergence within each physical step. Baldwin-Lomax [34], Baldwin-Barth [35] and Spalart-Allmaras [36] turbulence models were available. The code has been modified to solve multiple-block problems on a parallel architecture, and can handle deforming grids. However, the present investigation uses only single-block rigid grids. Numerous investigations have been performed with the solver, including dynamic stall [37], flapping-wing propulsion [9, 11], subsonic and transonic flutter [38], and limit-cycle transonic flutter [39–41].

Both Euler and Navier-Stokes simulations are run, with both high (10^6) and low (10^4) Reynolds numbers for the Navier-Stokes solutions. All solutions were run on a C-grid with 321×91 grid points, extending 10 chord lengths from the surface. Wall spacing was established so the value of y^+ was roughly 1.0 for the high Reynolds number cases. A surface detail of the grid is shown in Fig. 6. For the high Reynolds number Navier-Stokes simulations, fully turbulent flow is assumed at $\mathbf{M}_\infty = 0.3$, using the Baldwin-Lomax turbulence model. For the lower Reynolds numbers, fully laminar flow is assumed, and to get as close as possible to experimental conditions, the Mach number was lowered to 0.1.

FLOWer The finite volume code FLOWer was developed at the DLR Braunschweig (Deutsches Zentrum

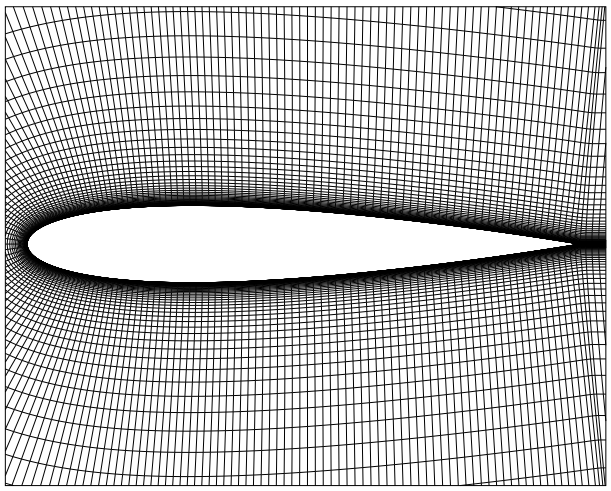

Fig. 6: NSTRANS 2D Navier-Stokes grid

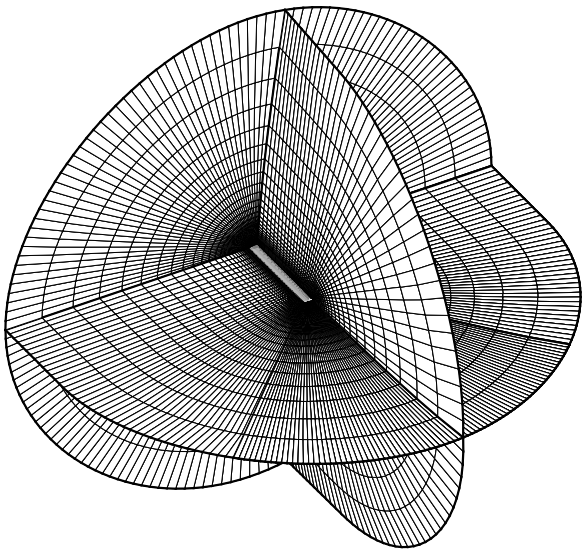

Fig. 7: Isometric view of the FLOWer 3D Euler grid, $A = 8$

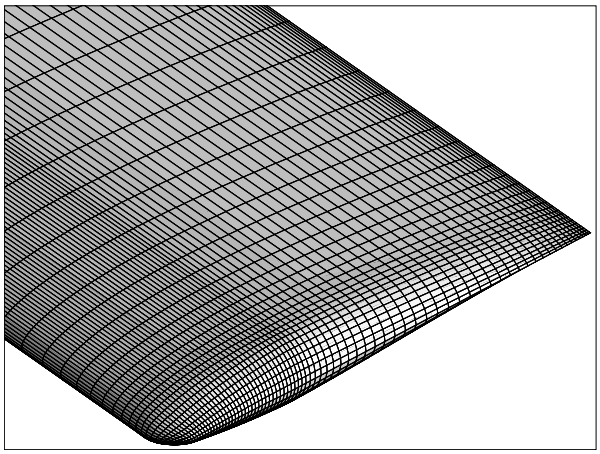

Fig. 8: Wing-tip detail of the FLOWer 3D Euler grid

für Luft- und Raumfahrt), Germany [42–44]. It solves the compressible, three-dimensional Euler and Navier-Stokes equations in integral form. A second-order, cell-vertex method for structured meshes discretizes the computational domain in space. Integration with respect to time is performed by means of a five-stage Runge-Kutta scheme to achieve converged solutions for both steady and unsteady flows. For the latter an implicit, dual time-stepping scheme [45], based on the method of Jameson [46], allows for the use of the same acceleration techniques which are used for steady-state flows, including implicit residual smoothing and a multi-grid scheme. An option for rigid body motions permits the calculation of flows around translating and rotating surfaces by specification of a single computational grid and the desired motion parameters. For more complicated wing movements the use of flexible meshes can be employed, as well as multiple block grids. However, the flapping motion used in this study can easily be handled by a single rigid grid. A variety of different turbulence models are implemented, including Baldwin-Lomax [34], Spalart-Allmaras [36] and Wilcox-k-ω [47].

The FLOWer code was employed for both two and three-dimensional simulations, providing an additional means of comparison with the NSTRANS code. For two-dimensional simulations a 321×65 O-grid was used, with a farfield boundary 50 chord lengths from the airfoil for Euler solutions, and 20 chord lengths from the airfoil for Navier-Stokes solutions. For three-dimensional Euler simulations a $121 \times 41 \times 49$ O-O-grid was used, and for Navier-Stokes simulations a $193 \times 57 \times 49$ O-O-grid was used, both with the outer boundary placed 10 chord lengths from the surface. Only half of the wing was modeled since the symmetry condition can be exploited. Details of the 3D Euler grid are shown in Figs. 7 and 8. The free-stream Mach number was set to 0.3 for all cases. For the Navier-Stokes calculations, fully turbulent flow was assumed using the Baldwin-Lomax turbulence model at $Re = 10^6$.

Calculations are performed using a local workstation and the super-computing facility HLRS in Stuttgart, Germany. Typically, three cycles are calculated requiring about 2 hours of CPU time for the 3D Navier-Stokes cases running on a single processor of a NEC SX-5 supercomputer, with 4GFLOP/s peak performance.

III. Results

The comparison of results for the wide variety of methods is mainly based on the evaluation of thrust

output and propulsive efficiency, which can be calculated from the time-dependent force coefficients. In addition, time-averaged and time-accurate results for horizontal wake velocities are shown. The difficulty in obtaining good agreement between experiment and numerics at low Reynolds numbers is highlighted using flow visualization.

Calculation of Thrust and Efficiency

In the wind-tunnel experiments it is difficult to isolate the drag created by the wing from the drag created by the rest of the model. Therefore, in order to facilitate comparisons with theory and the various numerical methods, the steady drag is removed from all experimental and numerical results. The mean thrust coefficient is therefore defined as

$$\overline{C}_T = -\overline{C}_D + C_{D\,\mathrm{stat}} \qquad (3)$$

where $\overline{C}_D$ is the mean drag coefficient, averaged for one flapping period. $C_{D\,\mathrm{stat}}$ is the steady drag of the non-moving wing at its present mean angle of attack. It can be easily determined in both experiment and numerical calculation prior to evaluating the flapping-wing results.

Defining the mean thrust coefficient according to Eq. (3) sets the focus solely on the effect of the flapping motion, since all forces from the static case are removed. Effectively, $\overline{C}_T$ only accounts for the forces due to the unsteady pressure distribution around the wing, since skin friction is nearly constant in time and thus equal in steady and unsteady case. This was verified with two- and three-dimensional Navier-Stokes results for the investigated parameter range at the high Reynolds number of 10^6.

The propulsive efficiency is calculated from the ratio between power output to power input. If dimensionless coefficients are used, this is equal to the ratio of mean thrust coefficient, $\overline{C}_T$, to mean power input coefficient, $\overline{C}_P$. The power input coefficient is calculated from the product of lift coefficient, C_L, and plunging velocity, $\dot{z}$.

Time-dependent Results for Thrust

Some time-dependent lift and thrust results are compared in Figs. 9 and 10 for $k = 0.4$ and $k = 0.2$, respectively. Integrating these coefficients over time yields the mean thrust and power coefficients, as described above.

In Fig. 9 the 2D and 3D panel-code results are shown illustrating the effect of aspect ratio. The 3D results rapidly approach the 2D results as A increases. With $A = 4$, the predicted thrust is about

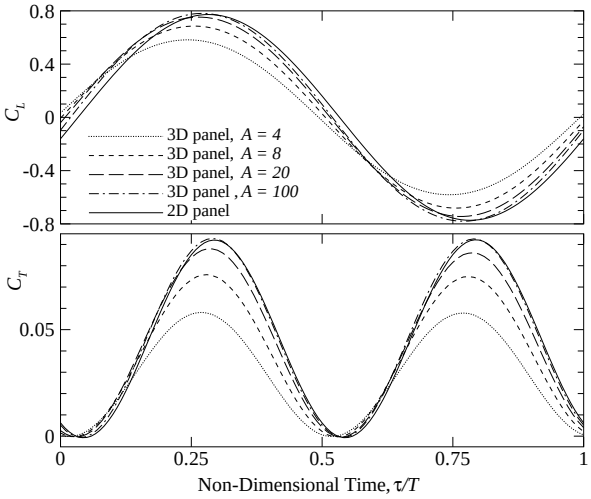

Fig. 9: Unsteady lift and thrust coefficient, $k = 0.4$

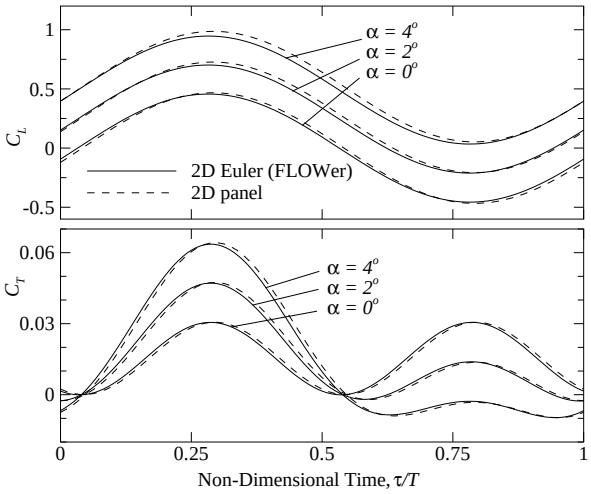

Fig. 10: Unsteady lift and thrust coefficient, $k = 0.2$

60 percent of the 2D result. At low aspect ratios, the usual unsteady phase lag in C_L and C_D vanishes due to the dominant tip vortices.

In Fig. 10, results for inviscid two-dimensional flows are compared. Agreement between Euler and panel results is good for all mean angles of attack shown. For increasing α, the thrust in the downstroke becomes stronger, while the thrust in the upstroke diminishes. However, for low amplitudes and frequencies, mean thrust output is essentially equal for all cases i.e. independent of the mean angle of attack. This was already suggested by Birnbaum [22] for deriving the two-dimensional theory for the thrust of an oscillating flat plate. However, the mean thrust remains independent of the mean angle of attack even in three-dimensional and vis-

cous flow, as long as the static drag at the considered mean angle of attack is eliminated according to Eq. (3) and no flow separation occurs. This was found to apply to all results obtained for this paper and consequently, no more results on the influence of the mean angle of attack are shown.

Comparisons for Thrust and Efficiency

The theoretical limit for the propulsive efficiency as k approaches zero is predicted with Eq. (2). In Fig. 11 the predictions of the theory for a two-dimensional flat plate, and the 2D and 3D panel code are compared. The agreement with the theoretical predictions is clear. Several factors may contribute to the discrepancy in the asymptotic value for $A = 4$; the wing-tip modeling, the assumed value of the induced-drag factor for the present wing planform, and numerical resolution difficulties at very low frequencies. Note that the 2D panel code, using the in-plane wake model, agrees exceptionally well with the theory, indicating that the primary weakness of the flat-plate theory is the planar wake representation.

In Fig. 12, the 2D and 3D results for $A = 8$ are shown, the trends are as expected. The results of all inviscid two-dimensional results (theory, panel, 2D Euler) are reasonably close. Also, 3D panel and 3D Euler results are in good agreement. The Euler results fall below the panel results due to the influence of compressibility.

From 2D to 3D, the efficiency drops due to the influence of the unsteady tip vortices, which form during the flapping cycle causing losses for the propulsive system. A difference in efficiency can also be found between inviscid and viscous flow calculations, although the static drag and thus the forces due to skin friction have been eliminated. However, the viscosity still affects the unsteady pressure distribution. As the wing experiences effective angles of attack different from zero throughout the cycle, the airfoil experiences an increase in pressure drag, which reduces the mean thrust output. This also leads to a decrease in efficiency.

For the lowest frequencies, however, the comparison becomes questionable. Here, the mean thrust output is low and in the same order of magnitude as the drag in the static case. Since the latter is subtracted to form the thrust coefficient defined in Eq. (3), the accuracy of the result comes into question. Moreover, both $\overline{C}_T$ and $\overline{C}_P$ tend toward zero, such that the propulsive efficiency becomes the ratio of two small numbers, and is consequently not very accurate.

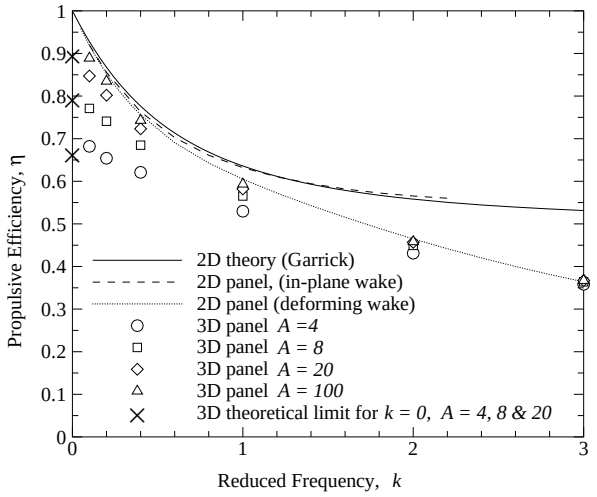

Fig. 11: Efficiency comparison for inviscid flow

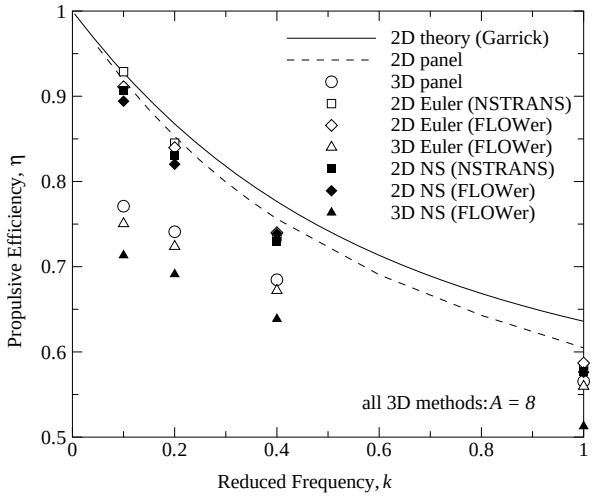

Fig. 12: Efficiency comparison for numerical methods

In the experiment, the evaluation of efficiency is rather difficult because this would require measuring the power input working against the aerodynamic forces. Mechanical losses in the flapping mechanism are very high, and very unsteady. Therefore, only the thrust output is measured with the laser range finder as mentioned previously. Different natural frequencies for flapping were tested at various tunnel speeds, resulting in a large number of data points for various reduced frequencies at different Reynolds numbers. An example for the raw data is shown in Fig. 13 for high aspect ratio and Reynolds number 4×10^4, where thrust is plotted against natural frequency. The mean values indicate the correct tendency, i.e. thrust is roughly proportional to the frequency squared. While the error in frequency

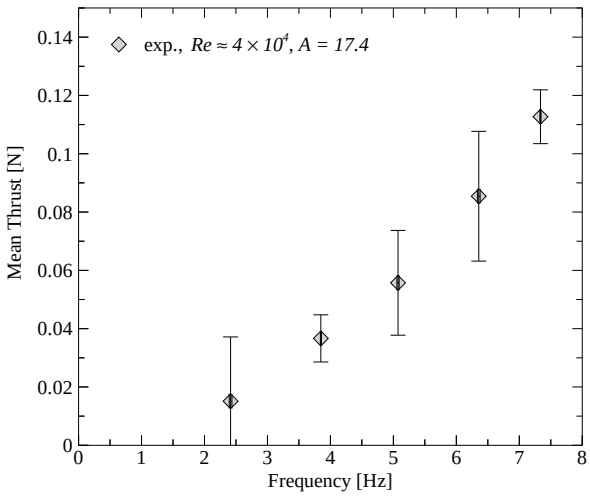

Fig. 13: Experimental data for mean thrust

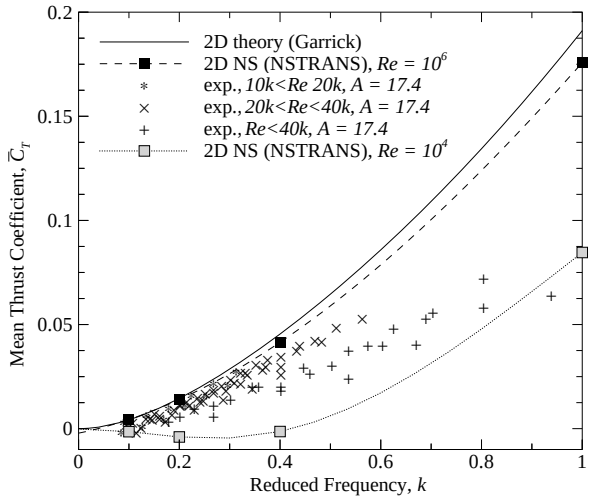

Fig. 14: Comparison of mean thrust coefficients

measurement is negligible, the deviation in thrust is quite high, primarily due to the model swinging at its natural frequency. For the remainder of the results, only the mean value is shown for the experimental results.

In Fig. 14 the predicted and measured thrust coefficients are shown. The experimental results cover a range of $10^4 < Re < 4.5 \times 10^4$. The data was obtained for a range of velocities between 2 and 9.5 m/s, and a frequency range between 2 and 7 Hz, and it is grouped into Reynolds number ranges to illustrate the trend. A high aspect ratio of 17.4 was investigated. For reference, the solid line gives the limit for the thrust coefficient if 3D effects and viscous effects are not included. All experimental data fall below this line, as they should. Additionally, all data points are nicely framed by the results for high and low Reynolds Number Navier-Stokes calculations for the two-dimensional case. The drop in thrust output from high to low Re is primarily due to dynamic stall, which is not predicted at the higher Reynolds numbers.

At $Re = 10^4$, periodic shedding occurs for the thick airfoil in the static case, which can be visualized in both experimental and numerical results. Fig. 15 shows streaklines from the smoke rake past the stationary wing at $Re = 10^4$. The smoke sheet is located at the middle of the half-span of the wing with aspect ratio 17.4. A street of alternating vortices is clearly visible in the wake, with a reduced shedding frequency of $k = 14.5$, measured using a strobe light. Similar results can be obtained with the Navier-Stokes solvers by means of particle tracing. Computed streaklines are visible in Fig. 16. For this result, the NSTRANS code was employed at $Re = 10^4$ and fully laminar flow, yielding excellent qualitative agreement with the flow pattern in

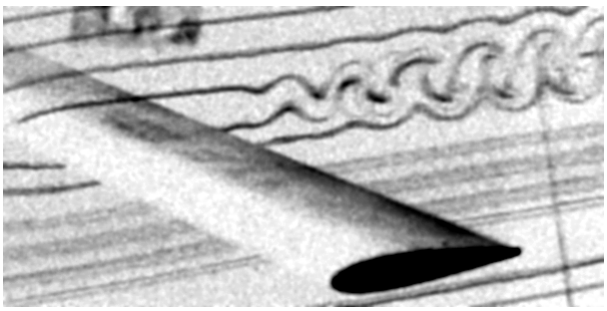

Fig. 15: Streaklines over non-moving wing, $Re = 10^4$

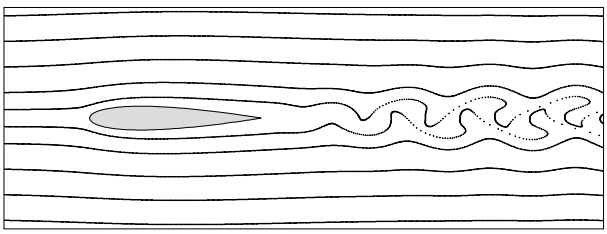

Fig. 16: Calculated streaklines (NSTRANS), $Re = 10^4$

the experiment. The calculated shedding frequency of $k = 12.3$ is somewhat lower than in the experiment. Using the airfoil thickness as the length scale, the Strouhal numbers for the experiment and simulation were 0.33 and 0.27, respectively, somewhat higher then the Strouhal number for the street behind a cylinder (0.21).

The numerical calculation of the steady shedding requires a relatively high temporal resolution and

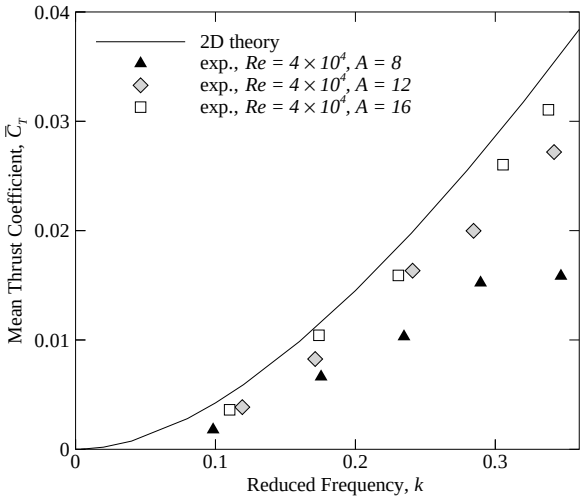

Fig. 17: Comparison of mean thrust coefficients

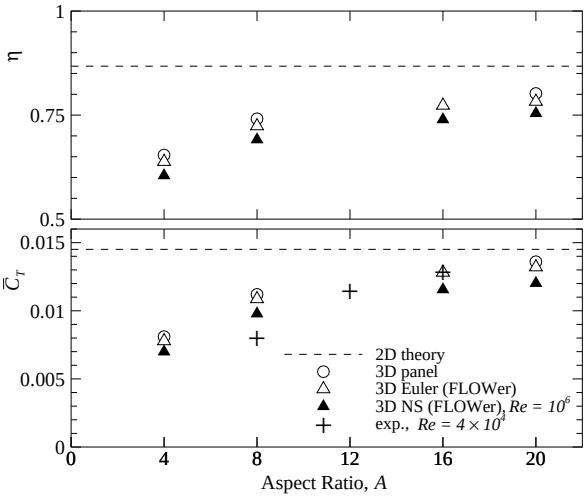

Fig. 18: Mean thrust coefficient and efficiency, $k = 0.2$

renders the application to flapping wing cases very costly in terms of computational effort. However, to capture the actual flow physics for the low Reynolds number regime, this becomes inevitable and is an open field for further research.

In three-dimensional flow, the aspect ratio has a strong influence on the thrust output of the flapping wing. As the span decreases, the influence of the tip vortices increase. Instantaneous vortices form during downstroke and upstroke causing an unsteady induced drag in both phases of the flapping cycle. This reduces thrust output and efficiency of the flapping wing which is shown by the experimental thrust coefficient results given in Fig. 17. As the flapping frequency increases, the influence of the tip vortices becomes more pronounced, since the wing is experiencing larger effective angles of attack during the flapping cycle. As a reference two-dimensional theory is given to indicate the theoretical limit. For high aspect ratios, the results tend towards this limit. This becomes more evident in Fig. 18, where numerical results for three-dimensional panel, Euler and Navier-Stokes calculations are included. Mean thrust coefficient and propulsive efficiency are shown as functions of aspect ratio. The experimental data for $k = 0.2$ was interpolated from the data in the Fig. 17. As expected, the larger aspect ratio wings help to increase the efficiency. While panel and Euler results for inviscid flow match quite well, the Navier Stokes results again show the influence of viscosity on the pressure distribution which reduces thrust and efficiency.

Wake Velocities

In Figs. 19 and 20, time-averaged velocity profiles one chord length downstream of the trailing-edge ($x = 2.0$) are compared for $k = 0.4$ and $k = 1.0$, respectively. Experimental data is measured with LDV half way between the fuselage of the model and the wing tip on the highest aspect-ratio wing. This is compared to the results computed by the 2D panel code and the 2D Navier-Stokes solvers. Only the U-component of the velocity is shown (only single-channel LDV was available).

In support of earlier experiments reported in Ref. [2], the panel code agrees quite well with the experiment. Note, the *uniform-flow* in the tunnel had an unfortunate gradient with respect to z of roughly 1 percent per chord-length, which was present with or without the model, and appears in all cases. While the Navier-Stokes results at $Re = 10^6$ agree well with panel code and experimental data, at the low Reynolds number a significant difference is apparent. At $Re = 10^6$ the jet-profile is fairly uniformly reduced due to viscous losses, but at low Reynolds numbers the viscous losses are much more substantial. It is difficult to judge from the rather sparse experimental data, particularly in the presence of the velocity gradient, but in Fig. 19 the width of the jet profile is comparable to the low Re results, but in Fig. 20, the width seems to agree more closely to the panel and high Re simulations.

In Figs. 21 and 22, unsteady LDV data is compared to the 2D panel and Navier-Stokes results for $k = 0.4$ and $k = 1$, respectively. The data is presented for three points located one chord length downstream of the trailing edge ($x = 2$), at $z = 1$, 0 and -1. The non-dimensional U-component of the velocity is shown as a function of the period.

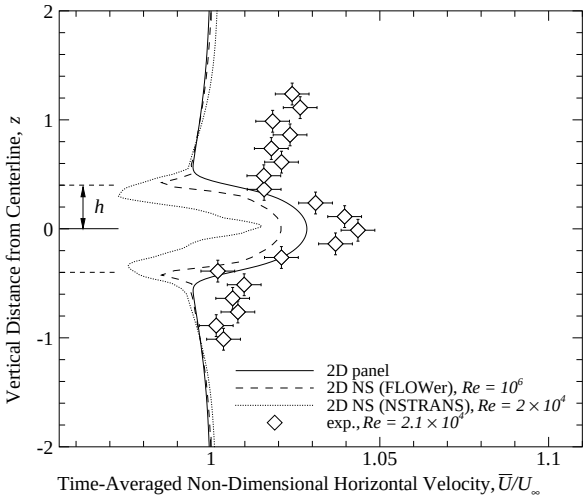

Fig. 19: Mean wake profile at $x = 2.0$, $k = 0.4$

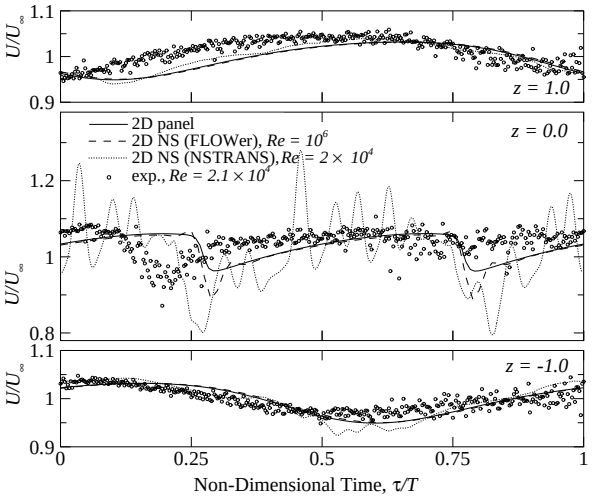

Fig. 21: Time-accurate U-velocity at $x = 2.0$, $k = 0.4$

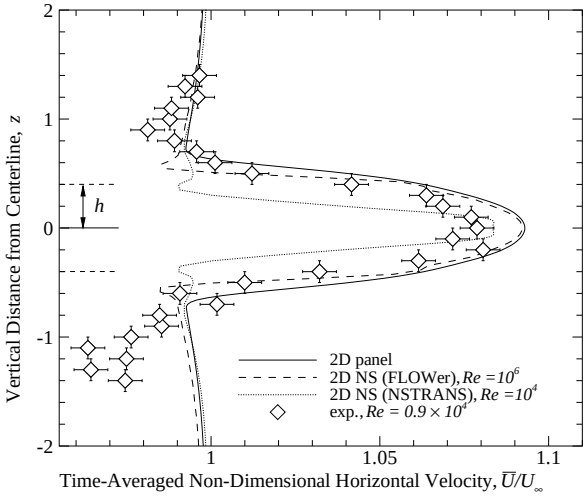

Fig. 20: Mean wake profile at $x = 2.0$, $k = 1.0$

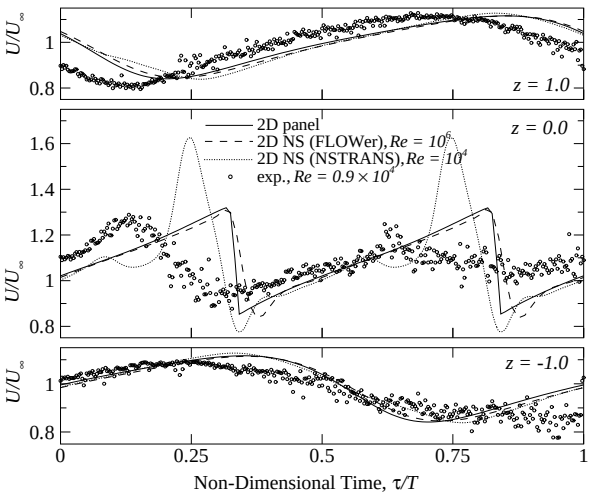

Fig. 22: Time-accurate U-velocity at $x = 2.0$, $k = 1$

The LDV data is accumulated over several minutes, so hundreds of cycles are essentially averaged. The LDV data becomes scattered in a few places, primarily for $z = 0$, as flow seeding is problematic in the wake region, resulting in rather sparse data.

Theoretically, the plots for $z = 1$ and $z = -1$ should be identical with a phase shift of half a period. This is apparent for the panel and Navier-Stokes results, and reasonably clear for the experimental data. For $z = 0$ the velocity should have twice the frequency of the flapping, so two periods should be visible. Again this is clear in the numerical results, and apparent in the experimental data.

The 2D panel code results and the high-Re Navier-Stokes results agree well, as do the NSTRANS result for $z = -1$ and 1. At the centerline ($z = 0$), the low Reynolds number Navier-Stokes results predict dynamic stall, with a series of vortices shed from the suction side, just past the midpoint in each stroke. The usual starting and stopping vortices shed from the trailing edge are not apparent, and while the vortex-street seen in the steady case (Fig. 15) is still visible through parts of the cycle, its influence on the velocities is negligible. Instead, the oscillatory behavior of the velocity apparent in the unsteady velocity at $z = 0$ is due to the sequence of dynamic stall vortices shed in the later half of each stroke. Figs. 23 and 24 show the vorticity distribution around the airfoil for reduced frequencies 0.4 and 1.0, respectively. The bottom line of the figures represents the centerline of the motion ($z = 0$). The flow field is cut off at $x = 2$, where the U-velocities

for the previous figures were taken. The airfoil is shown at the end of the upstroke ($t/T = 1$). Here, the dynamic stall vortices dominate the flow below the airfoil and, as they convect downstream, they eventually cause some additional oscillations in the horizontal velocity. The effect of these oscillations is clearly visible in the data at the centerline ($z = 0$) of the low Reynolds number data in Figs. 21 and 22. The slight departure from periodicity in these figures is most likely a result of the vortex-street seen in the steady results.

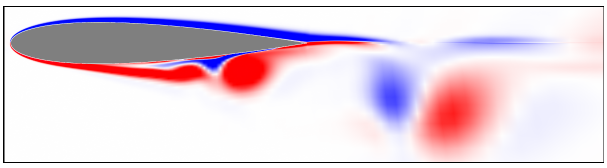

Fig. 23: Vorticity (NSTRANS), k=0.4, Re=2×10^4, τ/T=1

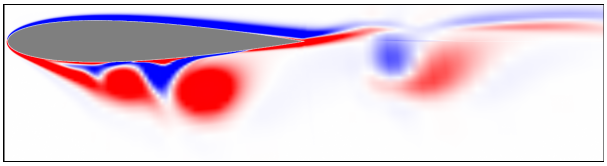

Fig. 24: Vorticity (NSTRANS), k=1, Re=10^4, τ/T=1

There is some uncertainty about the correct phasing of the experimental result in Figs. 21 and 22 relative to all other methods which agree quite well. There are various possible sources of error for the phase shift in the experiment. Canting and bending of the wing as well as vibrations of the whole model have an influence on the vertical position of the wing, which was not directly recorded in the experiment. Instead, the trigger signal, which indicates the onset of each flapping cycle, was thought to be sufficient for predicting the actual position of the wing. Note, however, that absolute velocity values are in excellent agreement for all methods. Also, a phase error does not affect the results of the preceding figures, since they only show time-averaged values.

IV. Summary

To evaluate thrust and efficiency for flapping wing configurations, a simple theory for two-dimensional, inviscid flow has been available for decades, but today computational fluid dynamics proves to be a valuable tool to also include viscous and three-dimensional effects in the calculation. The agreement between various numerical methods studied in this paper was encouraging and now provides a basis for subsequent authors. The influence of reduced frequency and aspect ratio on thrust output is further verified by the good agreement between experimental and numerical results. The experiment was carried out at low Reynolds numbers, below 5×10^4, which is still at the higher end of the range experienced in the flight of Micro Air Vehicles, where flapping wing propulsion may provide an alternative means for propulsion. In this regime, the flow physics are dominated by unsteady phenomena such as dynamic stall that introduce frequencies much higher than the actual flapping frequency. Further work is needed to bridge the gap between numerical results for high Reynolds numbers and the actual flight conditions, in particular, in the higher frequency regime where separation is a dominant feature.

V. Acknowledgments

The work at the Naval Postgraduate School was supported through the Naval Research Laboratory, under project monitors Kevin Ailinger, Jill Dahlburg and Jim Kellogg, and through the school's direct research program.

The work at the Institute of Fluid Mechanics in Braunschweig was funded by the DFG (German Research Foundation) as part of a graduate college. The research exchange with the Naval Postgraduate School in Monterey was made possible through a PhD scholarship grant from the DAAD (German Academic Exchange Service).

The authors would like to thank the Institute of Design Aerodynamics of the DLR Braunschweig, Germany, for providing the source code of the Euler/Navier-Stokes solver FLOWer as well as the grid generation tool.

VI. References

[1] Jones, K. D. and Platzer, M. F.: Numerical Computation of Flapping-Wing Propulsion and Power Extraction. AIAA Paper No. 97–0826, 1997.

[2] Jones, K. D; Dohring, C. M. and Platzer, M. F.: Experimental and Computational Investigation of the Knoller-Betz Effect. **AIAA Journal 36**, 1998, pp. 1240–1246.

[3] Jones, K. D. and Platzer, M. F.: An Experimental and Numerical Investigation of Flapping-Wing Propulsion. AIAA Paper 1999–0995, 1999.

[4] Lund, T. C.: A Computational and Experimental Investigation of Flapping Wing Propulsion, Master's thesis, Dept. of Aeronautics and Astronautics, Naval Postgraduate School, Monterey, CA, March 2000.

[5] Jones, K. D.; Platzer, M. F. and Lund, T. C.: Experimental and Computational Investigation of Flapping-Wing Propulsion for Micro Air Vehicles. Chapter 16, Fixed and Flapping Wing Aerodynamics for Micro Air Vehicle Applications, Mueller, T. J. (ed.), Progress in Astronautics and Aeronautics Series, AIAA, Reston VA, 2001, pp. 307–339

[6] Jones, K. D. and Platzer, M. F.: Flapping-Wing Propulsion for a Micro Air Vehicle. AIAA Paper 2000–0897, 2000.

[7] Duggan, S. J.: An Experimental Investigation of Flapping Wing Propulsion for Micro Air Vehicles. Master's thesis, Dept. of Aeronautics and Astronautics, Naval Postgraduate School, Monterey, CA, June 2000.

[8] Jones, K. D.; Duggan, S. J. and Platzer, M. F.: Flapping-Wing Propulsion for a Micro Air Vehicle. AIAA Paper 2001–0126, 2001.

[9] Tuncer, I. H. and Platzer, M. F.: Thrust Generation due to Airfoil Flapping. **AIAA Journal 34**, 1996, pp. 324–331.

[10] Tuncer, I. H.; Walz, R. and Platzer, M. F.: A Computational Study on the Dynamic Stall of a Flapping Airfoil. AIAA Paper 98-2519, 1998.

[11] Tuncer, I. H. and Platzer, M. F.: Computational Study of Flapping Airfoil Aerodynamics. **Journal of Aircraft 37**, 2000, pp. 514–520.

[12] Hummel, D.: The Aerodynamic Characteristics of Slotted Wing-Tips in Soaring Birds. In: Acta XVII Congressus Internationalis Ornithologici, Vol. 1, Nöhring, R. (ed.), Verlag der deutschen Ornithologen-Gesellschaft, 1978, pp. 391–396.

[13] Hummel, D.: The Use of Aircraft Wakes to Achieve Power Reduction in Formation Flight. AGARD CP-584, 1996, pp. 36–1 to 36–13.

[14] Hummel, D.: Aerodynamic Investigations on Tail Effects in Birds. **Zeitschrift für Flugwissenschaften und Weltraumforschung 16**, 1992, pp. 159–168.

[15] Hummel, D. and Möllenstädt, W.: On the Calculation of the Aerodynamic Forces Acting on a House Sparrow (Passer domesticus L.) During Downstroke by Means of Aerodynamic Theory. **Fortschritte der Zoologie 24**, 1977, pp. 235–256.

[16] Müller, J. and Hummel, D.: Time-Accurate CFD Analysis of the Unsteady Flow on a Fixed Delta Wing. AIAA Paper 2000–0138, 2000.

[17] Neef, M. F. and Hummel, D.: Euler Solutions for a Finite-Span Flapping Wing. Chapter 19, Fixed and Flapping Wing Aerodynamics for Micro Air Vehicle Applications, Mueller, T. J. (ed.), Progress in Astronautics and Aeronautics Series, AIAA, Reston VA, 2001, pp. 429-451

[18] Mahmoud, O. M. K. M.: Experimental Investigation of Low Speed Flow over Flapping Airfoils and Airfoil Combinations. Ph.D. thesis, Dept. of Aeronautics and Astronautics, Naval Postgraduate School, Monterey, CA, Sept 2001.

[19] Garrick, I. E.: Propulsion of a Flapping and Oscillating Airfoil. NACA Report No. 567, 1936.

[20] Theodorsen, T.: General Theory of Aerodynamic Instability and the Mechanisms of Flutter. NACA Report No. 496, 1934.

[21] Küssner, H. G.: Zusammenfassender Bericht über den instationären Auftrieb von Flügeln. **Luftfahrtforschung 13**, 1936, pp. 13:410–424,.

[22] Birnbaum, W.: Das ebene Problem des schlagenden Flügels. **Zeitschrift für Angewandte Mathematik und Mechanik 4**, 1924, pp. 277–292.

[23] Abbott, I. H. and von Doenhoff, A. E.: Theory of Wing Sections, Dover, New York, 1958.

[24] Teng, N. H.: The Development of a Computer Code for the Numerical Solution of Unsteady, Inviscid and Incompressible Flow over an Airfoil. Master's thesis, Dept. of Aeronautics and Astronautics, Naval Postgraduate School, Monterey, CA, June 1987.

[25] Jones, K. D. and Center, K. B.: Numerical Wake Visualization for Airfoils Undergoing Forced and Aeroelastic Motions. AIAA Paper 96–0055, 1996.

[26] Hess, J. L. and Smith, A. M. O.: Calculation of Potential Flow about Arbitrary Bodies. In: Progress in Aeronautical Sciences, Vol. 8, Pergamon Press, 1966, pp. 1–138.

[27] Basu, B. C. and Hancock, G. J.: The Unsteady Motion of a Two-Dimensional Airfoil in Incompressible Inviscid Flow. **Journal of Fluid Mechanics 87**, 1978, pp. 159–178.

[28] Ashby, D. L.; Dudley, M. R.; Iguchi, S. K.; Browne, L. and Katz, J.: Potential Flow Theory and Operation Guide for the Panel Code PMARC_12. NASA TM-102851, 1992.

[29] Garrison, P. and Pinella, D.: CMARC User's Guide. AeroLogic Inc., 1996.

[30] Ekaterinaris, J. A. and Menter, F. R.: Computation of Oscillating Airfoil Flows with One- and Two-Equation Turbulence Models. **AIAA Journal 32**, 1994, pp. 2359–2365.

[31] Chakravarthy. S. R. and Osher, S.: Numerical Experiments with the Osher Upwind Scheme for the Euler Equations. **AIAA Journal 21**, 1983, pp. 1241–1248.

[32] Osher, S. and Chakravarthy, S. R.: A New Class of High Accuracy TVD Schemes for Hyperbolic Conservation Laws. AIAA Paper 85-0363, 1985.

[33] Steger, J. L. and Warming, R. F.: Flux Vector Splitting of the Inviscid Gas Dynamic Equations with Applications to Finite-Difference Methods. **Journal of Computational Physics 40**, 1981, pp. 263–293.

[34] Baldwin, B. S. and Lomax, H.: Thin Layer Approximation and Algebraic Model for Separated Turbulent Flows. AIAA Paper 78-257, 1978.

[35] Baldwin, B. S. and Barth, T. J.: A One-Equation Turbulence Transport Model for High Reynolds Number Wall-Bounded Flows. NASA TM 102847, 1990.

[36] Spalart, P. R. and Allmaras, S. R.: A One-Equation Turbulence Model for Aerodynamic Flows. AIAA Paper 92–0439, 1992.

[37] Ekaterinaris, J. A. and Platzer, M. F.: Computational Prediction of the Airfoil Dynamic Stall. **Progress in Aerospace Sciences 33**, 1997, pp. 759–846.

[38] Jones, K. D. and Platzer, M. F.: Airfoil Geometry and Flow Compressibility Effects on Wing and Blade Flutter. AIAA Paper 98-0517, 1998.

[39] Weber, S.; Jones, K. D.; Platzer, M. F. and Ekaterinaris, J. A.: Transonic Flutter Computations for a 2D Supercritical Wing. AIAA Paper 1999–0798, 1999.

[40] Castro, B. M.; Ekaterinaris, J. A. and Platzer, M. F.: Transonic Flutter Computation for the NLR 7301 Airfoil Inside a Wind Tunnel. AIAA Paper 2000–0984, 2000.

[41] Castro, B. M.: Multi-Block Parallel Navier-Stokes Simulation of Unsteady Wind Tunnel and Ground Interference Effects. Ph.D. thesis, Dept. of Aeronautics and Astronautics, Naval Postgraduate School, Monterey, CA, Sept 2001.

[42] Radespiel, R.; Rossow, C. and Swanson, R. C.: Efficient Cell Vertex Multigrid Scheme for the Three-Dimensional Navier-Stokes Equations. **AIAA Journal 28**, 1990, pp. 1464–1472.

[43] Kroll, N.; Radespiel, R. and Rossow, C.-C.: Accurate and Efficient Flow Solvers for 3D Applications on Structured Meshes. In: VKI Lecture Series 1994-04 "'Computational Fluid Dynamics"', Brussels, 1994.

[44] Rossow, C.; Kroll, N.; Radespiel, R. and Scherr, S.: Investigation of the Accuracy of Finite Volume Methods for 2- and 3-Dimensional Flow. In: Validation of Computational Fluid Dynamics, AGARD CP-437, Vol. II, 1988, pp. P14–1 to P14–11.

[45] Heinrich, R. and Bleecke, H.: Simulation of Unsteady, Three-Dimensional Viscous Flows using a Dual-Time Stepping Method. In: New Results in Numerical and Experimental Fluid Mechanics, Contributions to the 10th AG STAB/DGLR Symposium, Braunschweig, 1996, pp. 173–180.

[46] Jameson, A. J.: Time Dependent Calculations Using Multigrid with Applications to Unsteady Flows Past Airfoil and Wings. AIAA Paper 91-1596, 1991.

[47] Wilcox, D. C.: Turbulence Modelling for CFD. DCW Industries Inc., 1998.

[48] Ghia, K. N.; Osswald, G. A. and Ghia, U.: Analysis of Two-Dimensional Incompressible Flow Past Airfoils Using Navier-Stokes Equations. In: Numerical and Physical Aspects of Aerodynamic Flows III, Cebeci, T. (ed.), Springer-Verlag, New York, 1986, pp. 318–338.